ACS OMEGA

Open Access

http://pubs.acs.org/journal/acsodf

Article

Nonadiabatic Coupling Dictates the Site-Specific Excited-State Decay Pathways of Fluorophenols

Jayshree Sadhukhan,* Moitrayee Mukherjee, Piyali Chatterjee, and Anwesha Datta

Cite This: *ACS Omega* 2025, 10, 7389−7399

Read Online

ACCESS | Metrics & More | Article Recommendations | Supporting Information

ABSTRACT: In this paper, a combined photophysical and electronic structure theory study demonstrating a remarkable site-specific fluorine substitution effect on the excited-state dynamics of monofluorophenols has been presented. The $S_1 \leftarrow S_0$ electronic origin band of phenol is shifted to a longer wavelength for *para* substitution, but to shorter wavelengths for *ortho* and *meta* substitutions. The observed sequence of excitation wavelengths of 2-fluorophenol (2FP) < 3-fluorophenol (3FP) < phenol < 4-fluorophenol (4FP) is consistent with the transition energies predicted by TDDFT/CAMB3LYP/6-311++G(d,p) and CASSCF-(8,8)/Dunning cc-pVDZ theoretical methods. The most notable contrast of excited-state dynamics is revealed in the different features of the fluorescence spectra; the fluorescence yield of 4FP is almost 6 times larger compared to that of 3FP and the spectral bandwidth of 2FP is nearly 1.5 times larger than that of 4FP. Electronic structure calculation predicts a low-energy S_1/S_0 conical intersection (CI) near the $^1\pi\pi^*$ minimum with respect to the prefulvenic vibronic mode of the aromatic ring, and the energetic location of this CI is altered with the substitution site of the fluorine atom. The predicted energy barrier to this prefulvenic CI is smallest for 3FP but largest for 4FP, leading to a facilitated nonradiative electronic relaxation of the former (3FP), and emission occurs with a much diminished fluorescence intensity.

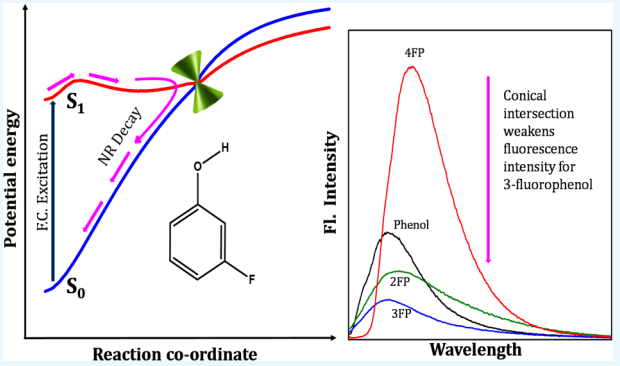

1. INTRODUCTION

The excited-state relaxation dynamics and photochemistry of molecules in the framework of nonadiabatic dynamics have drawn a surge of interest from both theoretical and experimental perspectives in the past couple of decades.[1−22] The close proximity of the molecular electronic potential energy surfaces, which is common in polyatomic molecules, results in breakdown of the Born-Oppenheimer approximation.[1] As a result, vibronic mixing among the states allows the nuclei to move concurrently on multiple electronic surfaces, which leads to the generation of conical intersections (CIs) among the states and introduces quantum mechanical tunneling as one of the intriguing phenomena in the excited-state dynamics of polyatomic molecules.[2−22] Such interactions significantly raise the propensity of nonradiative decay of the molecular excited electronic states and leave footprints of the effects in the electronic absorption and fluorescence spectra.[23−33] Photophysical interpretations in terms of interplay between the low-lying excited electronic states have previously been provided for phenol, substituted phenols, and other photoacid molecules like pyrrole, indole, and substituted indoles.[34−40] The photophysical and photochemical studies of fluorinated aromatic compounds have drawn significant attention from theoretical and experimental researchers.[41−46]

Phenol, the smallest aromatic alcohol, is the light-absorbing chromophore of the aromatic amino acid tyrosine that plays a vital role in photosynthetic processes.[47] This chromophore is also a simple photoacid molecule and its acid dissociation constant is increased by nearly 6 orders of magnitude upon UV excitation.[48] Many photophysical studies have been carried out in the recent past with this molecule and its hydrogen-bonded complexes with water and ammonia in gas phase, as well as in condensed media of different polarities.[49−61] The key photophysical effects of the nonadiabatic coupling among the low-lying excited electronic states of isolated phenol are the low quantum yield of fluorescence, relatively fast excited-state decay, and detachment of the H atom from the phenolic O−H group.[61] It has been suggested that the same mechanism is responsible for the ultrafast electronic relaxations of the purine and pyrimidine bases of the nucleic acids and offers photostability to many important biomolecules in the natural environment.[62−66]

A unique underlying mechanism that governs the excited-state dynamics of this class of molecules, as mentioned above,

Received: December 16, 2024
Revised: January 16, 2025
Accepted: January 23, 2025
Published: February 15, 2025

is the interplay between the optically bright $^1\pi\pi^*$ and the dissociative $^1\pi\sigma^*$ states.[67−74] For phenolic systems, a CI is developed between the two excited states at ∼1.2 Å length of its O−H bond.[26] At a still longer O−H distance, a second CI results between the $^1\pi\sigma^*$ and S_0 states.[26] For phenol, the first CI between the $^1\pi\sigma^*(S_2)$ and $^1\pi\pi^*(S_1)$ states is located near 5.0 eV, which is ∼0.5 eV above the energy minimum of the S_1 state.[23,28] When the excitation energy exceeds the S_1/S_2 CI energy, typically at a wavelength shorter than 240 nm, the O−H bond fission may occur within a few hundred femtoseconds.[75] But for excitations below the CI barrier, O−H bond fission is slower compared to other electronic relaxation processes.[75] However, the possibility of tunneling-mediated O−H bond fission in nanosecond time scale has been discussed in the recent literature.[75] In addition, a "channel-three" S_1/S_0 radiationless decay pathway involving the prefulvenic isomeric mode for the single-ring aromatic systems was also proposed.[76−78,23,80] This nonradiative channel opens up at 3000 cm^{-1} above the S_1 ($\pi\pi^*$) origin for benzene.[76−78] For phenol, the barrier height for this channel is reported to be 6370 cm^{-1} above the S_1 minimum.[23] It is shown here that this S_1/S_0 CI is indeed the key mechanism for the site-specific excited-state decay of the fluorine-substituted phenols considered in the present study.

Recently, Sage et al. studied the *para* halogen substitution effects on the photodissociation dynamics of phenol and identified a competition between O−H and C−Y (Y = Br/I) bond fissions in 4-bromophenol and 4-iodophenol upon excitations in the wavelength range of 215−330 nm.[79] For 4-chloro and fluorophenols, no Cl and F atoms have been identified, and O−H bond fission is considered as the primary photodissociation channel of these two molecules. Harris et al. recognized a completely different ultrafast S_1 state relaxation dynamics for 2-chlorophenol that matches well with its subpicosecond S_1 state lifetime, while for 3- and 4-chlorophenols, the lifetimes are ∼3 and ∼4 orders of magnitude longer and in the nanosecond time scale.[80] They proposed the occurrence of the fast IC for the 2-substituted phenols involving the C−Cl stretching coordinate owing to the intramolecular O−H···Cl hydrogen bonding, which could stabilize the $^1\pi\sigma^*$ energy state, leading to a barrierless IC to the ground state. However, the same does not occur for 2FP and the S_1 state lifetime was measured to be in the nanosecond time scale.[75] Pino et al. have reported the experimentally measured S_1 state lifetime for 2FP, 3FP, and 4FP as 4.6 ns, 1.9 ns, and 1.8 ns, respectively, under the isolated condition in the gas phase.[22]

The studies presented above underlie the fact that the information about the energetics of CI points and the corresponding geometries are important parameters to explain the photophysical and photochemical behaviors of phenolic and analogous systems.[81−85] While the use of a multireference theoretical method is recognized to be the most powerful approach for quantitative prediction in this regard, its limited applicability for medium to large-sized molecules calls for a less computationally demanding method, and the time-dependent density functional theory (TDDFT) is proposed and tested to be a practical approach in this regard. Earlier, Robinson and co-workers have drawn a comparison of the spin-flip TDDFT minimal energy crossing point CI approaches with the extended multistate complete active-space second-order perturbation theory (XMS-CASPT2) for a large class of molecules like fulvene, 5-fluorocytosine, 9*H*-adenine, azomethane, azoxymethane etc.[86] Levine et al. showed that under certain approximations, the TDDFT method can satisfactorily predict minimum energy CI (MECI) geometries and energetics.[87] Filatov explored the impact of the choice of density functional on MECI geometries in comparison with various multireference approaches like the complete active-space self-consistent field (CASSCF) and CASPT2.[88] Olivucci and co-workers compared TDDFT//CASSCF calculations with the more expensive CASPT2//CASSCF level for evaluation of the excited-state isomerization pathway of retinal chromophores.[89] Excited-state proton transfer (ESPT) and photoinduced electron transfer (PET) have extensively been studied using TDDFT methods.[90,91] Truhlar and co-workers assessed the performance of the M06 family of functionals for prediction of electronic excitation energies by TDDFT methods and found the M06-L functional as the most efficient one in prediction of the excitation energies among other similar functionals.[92]

In this work, we report a combined photophysical experimental and computational study of the three monofluorophenols, 2FP, 3FP, and 4FP, to investigate the site-specific substitution effects on the electronic relaxation dynamics following $^1\pi\pi^*$ excitation. The results presented below show that the effects are quite distinct. The interpretation of the findings given is based on the predictions of the electronic structure theory calculations. Although fluorine atoms are weak hydrogen bond acceptors, the presence of weak O−H···F hydrogen bonding in 2FP has been evidenced in a recent infrared spectroscopy study under an matrix isolation condition and also by the use of photoionization mass spectrometry.[93] The effect of the site-specific substitution of the fluorine atom on the structure and dynamics of such molecules is the primary focus of this study.

2. EXPERIMENTAL AND THEORETICAL METHODS

Phenol (purity >99.0%), 2FP (purity >99.0%), 3FP (purity >99.0%), and 4FP (purity >99.0%) were purchased from Sigma-Aldrich and used as supplied. UV-grade methylcyclohexane (MCH), used as a solvent in the present study, was procured from Spectrochem India Pvt. Ltd. and used as supplied after confirming that it had no fluorescent impurity. For recording the absorption and fluorescence spectra, a 1×10^{-4} M solution of each compound was prepared in MCH. At room temperature, the electronic absorption spectra of all of the solutions were measured using a Shimadzu UV spectrometer (model 2410) and the fluorescence spectra of the same sets of solutions were recorded using a spectrofluorimeter, make JobinYvon, model- FluoroMax-3.

For the reference equilibrium geometries of all of the four molecules in the ground state (S_0), geometry optimization was carried out at the second-order Møller−Plesset perturbation (MP2) level using the 6-311++G(d,p) basis set employing the GAUSSIAN 09 package.[94] All of the optimized ground-state geometries converged to the C_s symmetry point group. Starting from these reference geometries, the electronic structure calculations for the low-lying excited electronic states and CIs were carried out using the correlation-consistent polarized valence double-ζ basis set (Dunning cc-pVDZ) at the state-averaged CASSCF level using the GAMESS package.[95]

The active space used for CASSCF calculations of phenol, CAS(8,8), refers to three phenyl ring-centered π orbitals, an O(2px)-conjugated lone pair orbital, three ring-centered π^* orbitals, and an O−H antibonding σ^* orbital. For fluorophe-

https://doi.org/10.1021/acsomega.4c11321
ACS Omega 2025, 10, 7389−7399

nols, a fluorine-conjugated lone pair orbital was incorporated into the active space. Alongside, the ground-state geometry optimizations were carried out using the density functional theory (DFT)/Coulomb-attenuating method by employing Becke three-parameter hybrid functionals and the correlation functional of Lee, Yang, and Parr (CAMB3LYP) using the 6-311++G(d,p) basis set, and the calculations for the corresponding excited states were performed at the TDDFT/CAMB3LYP/6-311++G(d,p) level using GAMESS package.[95] The solvent effects for the same were taken into account by using the integral equation formalism of the polarizable continuum model (IEFPCM).[96] The vertical excitation energies (VEEs) of $^1\pi\pi^*$ and $^1\pi\sigma^*$ electronic states were calculated corresponding to the ground-state equilibrium geometries using CASSCF/Dunning cc-pVDZ method implemented in the GAMESS suite of programs.[95]

The natural bond orbital (NBO) dipole moment calculations and the electronic structure calculation of the potential energy curves (PECs) of the S_0 ($\pi\pi$), S_1 ($\pi\pi^*$), and S_2 ($\pi\sigma^*$) states with C_s symmetry constraint were performed along the O−H stretching coordinate at the TDDFT/CAMB3LYP/6-311++G(d,p) level of calculation. The CI points for phenol and fluorophenols were also optimized at the CASSCF(8,8)/Dunning cc-pVDZ level using the CI search algorithm implemented in the GAMESS program package.[95] The barrier heights to these CIs from the respective minimum energy structures of the S_1 states were computed here to provide an understanding and interpretation of the experimental absorption and fluorescence spectra.

3. RESULTS AND DISCUSSION

3.1. Absorption Spectra and Low-Lying Electronic States of Fluorophenols. The ultraviolet absorption spectra of phenol, 2FP, 3FP, and 4FP in MCH solutions (1×10^{-4} M) within the wavelength range of 240−320 nm are presented in Figure 1. These absorption spectra shown in Figure 1 correspond to the $S_1 \leftarrow S_0$ vibronic transitions of phenol, 2FP, 3FP, and 4FP. The longest wavelength peaks in these spectra representing the electronic origin bands of these molecules appear in the following order—2FP (273.8 nm) < 3FP (274.4 nm) < phenol (277.6 nm) < 4FP (287.6 nm), with absorbance values of 0.134, 0.114, 0.131, and 0.234, respectively. The comparison implies that the $S_1 \leftarrow S_0$ energy gap of phenol in MCH is increased upon fluorine substitution at 2- and 3-position of the ring, but it is reduced for the same substitution at 4-position, and the same sequence trend is recorded for the spectra under the jet cooling condition. The $S_1 \leftarrow S_0$ electronic origin bands under the latter condition appear at 284.7 nm, 275.1 nm, 273.0 nm, and 271.7 nm for 4FP,[101] phenol,[99] 3FP,[18] and 2FP,[100] respectively. It is noteworthy that in each case, the $S_1 \leftarrow S_0$ electronic origin band is shifted to a longer wavelength for the condensed phase in comparison with those of the supersonic jet expansion condition, and this can be demonstrated as a direct evidence of the solvent-induced excited-state stabilization phenomenon that effectively lowers $S_1 \leftarrow S_0$ energy spacing. The extent of shift from the gas to solution phase can be directly correlated to the ground-state dipole moment of the molecules. The shift is maximum (2.9 nm) for 4FP, the most polar molecule among the four molecules, and minimum (1.4 nm) for the least polar 3FP molecule. The observed sequence can be explained in the following way. The F atom exerts an electron-withdrawing inductive effect, which is more effective at 2- and 3-positions.

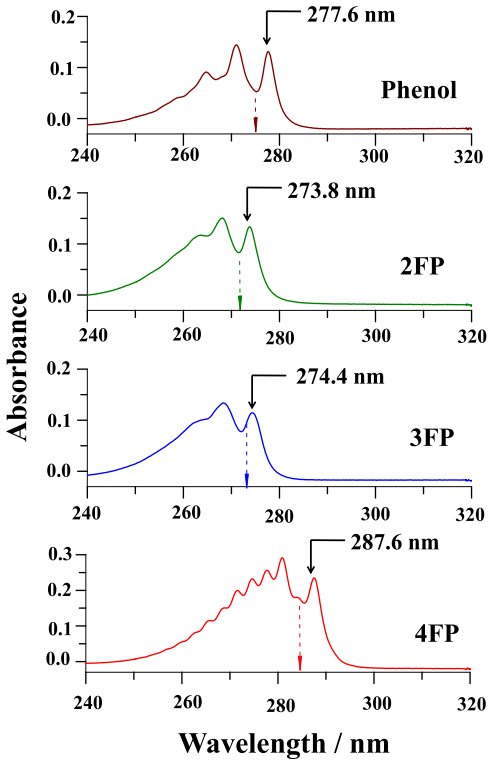

Figure 1. UV absorption spectra of 1×10^{-4} M solutions of phenol, 2FP, 3FP, and 4FP in MCH at room temperature. The wavelength at the absorption maximum of the first band is displayed in each case. The corresponding wavelengths for the $S_1 \leftarrow S_0$ electronic origin bands of the jet-cooled molecules are shown by dotted arrows.[18,99−101]

The electron-releasing mesomeric effect is effective dominantly for substitution at the 4-position. It is also noteworthy that the finer vibronic structures in the UV absorption spectra, which are primarily for the in-plane deformation modes of the aromatic ring, appear prominent in the case of 4FP only. However, these features are relatively broader in the spectra of 2FP and 3FP. Such differences in vibronic features, which are apparent even in solutions at room temperature, indicate that the ring turns out to be more rigid on *p*-fluorine substitution, but the rigidity is diminished for substitutions at 2- and 3-sites of the ring.

The vertical and adiabatic electronic excitation energies for the lowest-energy transitions calculated for phenol, 2FP, 3FP, and 4FP at TDDFT/CAMB3LYP/6-311++G(d,p) and CASSCF/Dunning cc-pVDZ levels are presented in Table 1. The predictions of both levels of calculation correlate well with the experimental trends of the $S_1 \leftarrow S_0$ band origins. The vertical excitation energies for the lowest-energy transitions calculated for phenol, 2FP, 3FP, and 4FP at the TDDFT/CAMB3LYP/6-311++G(d,p) level in the IEFPCM model appear at 5.215 eV, 5.283 eV, 5.272 eV, and 5.027 eV, respectively. It clearly reflects a similar trend for the $S_1 \leftarrow S_0$ electronic origin bands in the MCH solvent with that of the gas-phase condition and points toward the longer wavelength shift of the electronic origin band for the condensed phase caused by the solvent-induced excited-state stabilization phenomena. The oscillator strength values for the $S_1 \leftarrow S_0$ transitions predicted by TDDFT/CAMB3LYP/6-311++G-(d,p) methods are 0.0350, 0.0303, 0.0244, and 0.0632 for phenol, 2FP, 3FP, and 4FP, respectively. The S_1−S_0 transition

https://doi.org/10.1021/acsomega.4c11321
ACS Omega 2025, 10, 7389−7399

Table 1. Vertical and Adiabatic Excitation Energies (in eV) for $S_1 \leftarrow S_0$ Electronic Transitions of Phenol, 2FP, 3FP, and 4FP Predicted by TDDFT/CAMB3LYP/6-311++G(d,p) and CASSCF/Dunning cc-pVDZ Theoretical Methods and Those Obtained Experimentally

	$S_1 \leftarrow S_0$ vertical energy/eV		$S_1 \leftarrow S_0$ optimized energy/eV		experimental energy/eV	
	CAMB3LYP/6-311++G(d,p)	CAS(8,8)/Dunning cc-pVDZ	CAMB3LYP/6-311++G(d,p)	CAS(8,8)/Dunning cc-pVDZ	in gas phase	previously calculated energy/eV
phenol	5.343	4.857	5.070	4.814	4.506[a]	4.864(4.673)[e]
						4.759(4.612)[f]
						4.455(4.308)[f]
						4.816(4.669)[f]
						4.869[g]
						4.52(4.37)[h]
2FP	5.400	4.931	5.050	4.882	4.562[b]	4.932(4.677)[e]
3FP	5.399	4.909	5.108	4.830	4.541[c]	4.917(4.715)[e]
4FP	5.198	4.835	4.860	4.803	4.355[d]	4.668 (4.462)[e]

[a]Ref 98. [b]Ref 99. [c]Ref 18. [d]Ref 100. [e]CC2/aug-cc-pVDZ level ref 22. [f]CAS(10,9)/6-31G**; MRMP2/6-31G**; MRCI/aug-cc-pVDZ levels ref 23. [g]EOM-CCSD/aug-cc-pVTZ level ref 85. [h]CASSCF(10/10)/aug(O)-AVTZ//CASPT2(10/10)/aug(O)-AVTZ level ref 103.

dipole moments are calculated to be 1.3137 D, 1.2158 D, 1.0920 D, and 1.7899 D for phenol, 2FP, 3FP, and 4FP, respectively, and they are confined to the ring plane for all of the molecules at the TDDFT/CAMB3LYP/6-311++G(d,p) level of calculations. The transition dipole moment trend for phenol, 2FP, 3FP, and 4FP aligns with the trend of oscillator strengths, which eventually correlates with the integrated absorbance. Since the absorption arises from an electronic transition, the oscillator strength value quantifies the absorption intensity and it is directly proportional to the absorption area.[102] The ratio of the predicted oscillator strengths for 4FP and 3FP is ~2.6, which is quite consistent with the oscillator strength ratio of the same calculated from the integrated absorbance of the experimental spectra of ~2.3.

The predicted energy ordering of the $^1\pi\pi^*$ and $^1\pi\sigma^*$ electronic states following vertical excitation from the respective S_0 states of phenol, 2FP, 3FP, and 4FP, calculated at CASSCF/Dunning cc-pVDZ level are shown schematically in Figure 2. These predictions for phenol are in excellent agreement with those reported by Mahapatra and co-workers for calculations performed at the EOM-CCSD level using MOLPRO.[85] Shown also are the $^1\pi\pi^*$ state energies obtained from experiments in the gas phase (dotted lines); the predicted energy ordering for this state is in good agreement with the observation. Interestingly, for the $^1\pi\sigma^*$ state, the F substitution effect at the *para*-position is predicted to be distinctly opposite to the energy lowering of the $^1\pi\pi^*$ state. It is shown below that such an increase of the $^1\pi\sigma^*$ state energy of 4FP affects the excited-state dynamics and photophysical manifestation of the molecule.

3.2. Fluorescence Spectra and Excited-State Geometries. The fluorescence spectra of phenol, 2FP, 3FP, and 4FP in MCH solution (1×10^{-4} M) upon excitations at 268 nm are displayed in Figure 3. It has been ensured that the absorbance values at this excitation wavelength are almost the same for all fluorophenols. The Stokes shifts between the fluorescence maxima (Figure 3) and the longest wavelength peak (electronic origin band) of the $S_1 \leftarrow S_0$ absorption

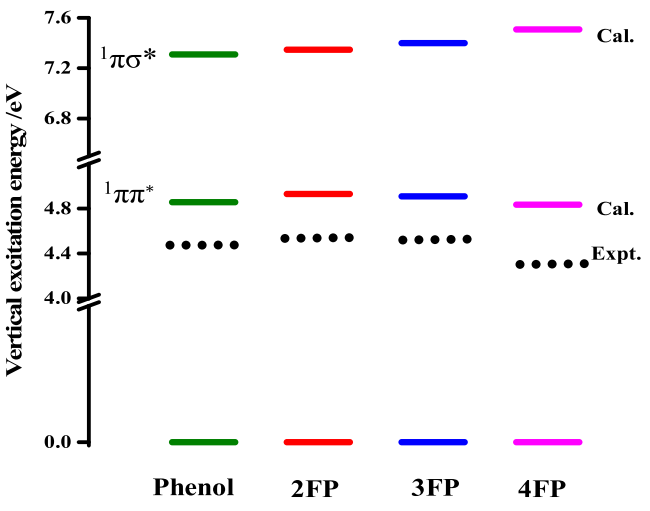

Figure 2. Energy ordering of $^1\pi\pi^*$ and $^1\pi\sigma^*$ excited electronic states of phenol, 2FP, 3FP, and 4FP calculated for the ground-state equilibrium geometries at CAS(8,8)/Dunning cc-pVDZ level. The corresponding experimental $^1\pi\pi^*$ energy state values obtained from experiments in the gas phase are denoted using black dotted lines.

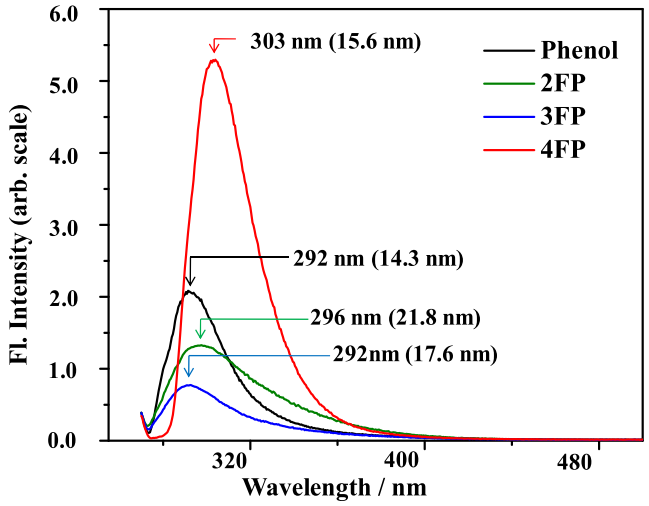

Figure 3. Fluorescence spectra of solutions of phenol, 2FP, 3FP, and 4FP in MCH at room temperature upon excitation at 268 nm. The concentrations of all of the compounds in the respective solutions are the same, 1×10^{-4} M. The extent of Stokes shift has been indicated within parentheses in each case.

https://doi.org/10.1021/acsomega.4c11321
ACS Omega 2025, 10, 7389−7399

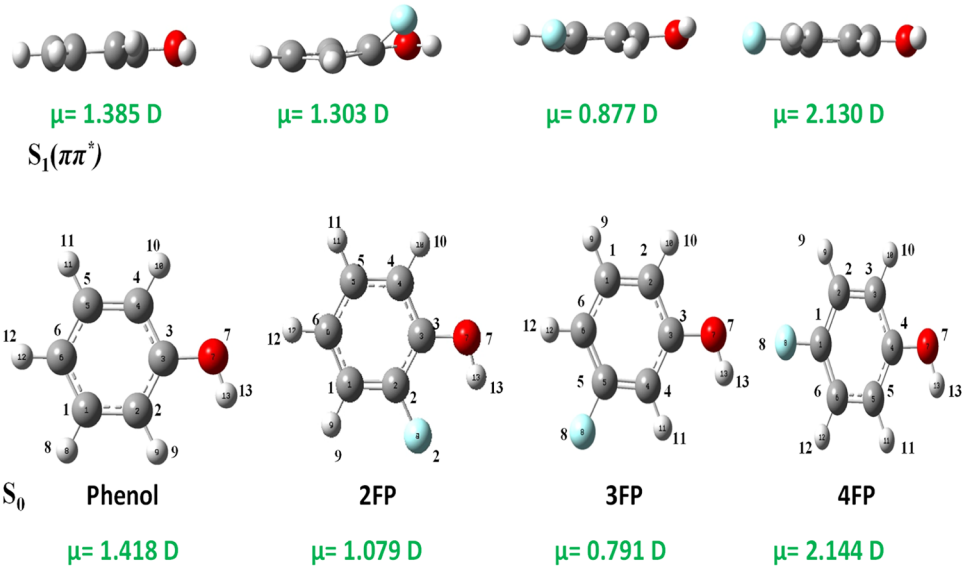

Figure 4. Optimized geometries of phenol, 2FP, 3FP, and 4FP at DFT/CAMB3LYP/6-311++G(d,p) for S_0 state and TDDFT/CAMB3LYP/6-311++G(d,p) for S_1 state. The dipole moment values for each one calculated at the same level are also mentioned.

spectra (Figure 1) in each case is the least for phenol, only 14.3 nm, but the same is maximum for 2FP (21.8 nm). The shifts for 3FP and 4FP are 17.6 nm and 15.6 nm, respectively. The notable contrasts are displayed with respect to fluorescence intensity as well as the full width at half-maximum (FWHM) of the fluorescence bands. While the bandwidth (FWHM) of 2FP is the largest (50.1 nm), the fluorescence yield of 4FP is relatively large and almost 5.6 times larger than that of 3FP. This finding vividly depicts that the photophysical processes in the excited state are sensitively dependent on the fluorine substitution site of the aromatic ring.

The optimized geometrical parameters in S_0 and $S_1(\pi\pi^*)$ states for calculations at CASSCF(8,8)/Dunning cc-pVDZ and TDDFT/CAMB3LYP/6-311++G(d,p) levels are presented in Tables S1, S2, S3, and S4 for phenol, 2FP, 3FP, and 4FP, respectively (Supporting Information, SI). A pictorial representation of the dominant changes of the structures for $S_1(^1\pi\pi^*) \leftarrow S_0$ excitation of all four phenols, as predicted by the TDDFT method, is shown in Figure 4. A scrutiny of the structures reveals that the geometric distortion in S_1 is minimum for 4FP followed by phenol, and the two molecules fairly retain the ground-state planarity in the $S_1(\pi\pi^*)$ state. In contrast, 3FP suffers major skeletal distortions upon $\pi\pi^*$ excitation and 2FP shows prominent out-of-plane distortion of the *ortho*-fluorine atom in the S_1 state, where the fluorine atom does not remain in the ring plane and the change of O7−C3−C2−F8 dihedral angle is ∼38°. The predicted changes are quite consistent with the previous report of Zhang and co-workers, where the S_1 minima for 2FP is calculated to be nonplanar with the fluorine atom rotated by 37° out-of-the aromatic plane.[97] On the other hand, in the case of 3FP, the TDDFT calculation predicts that the *ortho*-H atom, which is labeled as H11 (Figure 4), suffers a major angular distortion, as evidenced by the change of O7−C3−C4−H11 dihedral angle by ∼21° in the S_1 state compared to that of S_0, and the aromatic ring is significantly deformed from planarity. Summarily, upon photoexcitation to the S_1 state, 4FP and phenol show minimal geometric distortions, but for the other two, the extents of geometrical distortions are significantly large.

The structural distortions observed in the excited states of 2FP and 3FP suggest that their ground-state geometries are significantly different from those of the energy minima in the $^1\pi\pi^*$ states. This shift in geometry is responsible for the relatively broad fluorescence spectrum of 2FP compared to that of 4FP (Figure 3). In contrast, 4FP, which benefits from high resonance stabilization due to extended conjugation, maintains structural planarity upon $^1\pi\pi^*$ excitation. Therefore, the geometry in the S_1 minimum is likely very similar to the S_0 geometry. As a result, the Stokes shift between the absorption and emission maxima of 4FP is minimal, resembling that of phenol. Moreover, the effect of such geometry changes is also evident in the $S_1 \leftarrow S_0$ electronic absorption band, as discussed in the previous section in terms of difference in longest wavelength absorption peak, integrated absorbance, and appearance of vibronic structures in the UV absorption spectra for phenol, 2FP, 3FP, and 4FP.

3.3. Excited-State Dynamics. Displayed in Figure 5 are the cuts through the potential energy profiles of the S_0 ($\pi\pi$), S_1 ($\pi\pi^*$), and S_2 ($\pi\sigma^*$) states of phenol, 2FP, 3FP, and 4FP as a function of their O−H stretching coordinate according to the predictions of TDDFT/CAMB3LYP/6-311++G(d,p) level of calculation with C_s symmetry constraint. All of these adiabatic potential energy curves (PECs) are obtained by progressively scanning along R_{O-H} with geometry relaxation for individual S_0, S_1, and S_2 states, while all of the atoms are constrained to remain in a plane. In agreement with the report of Domcke and co-workers, the plots shown in Figure 5 indicate that the S_1 and S_2 PECs of phenol give rise to a CI at R_{O-H} ∼1.2 Å and a second CI with that of the ground state (S_0) upon further stretching of the O−H bond.[26] At C_s symmetric geometries, the magnitude of the energy barrier along S_1/S_2 CI relative to the S_1 minimum of phenol predicted by the method used here is similar to that reported in ref 26, and, further, the values are almost the same for all monofluorophenols. Thus, it is unlikely that the interelectronic state coupling with respect to simple O−H bond elongation could be adequate to explain nearly an order of magnitude difference in fluorescence yield between 3FP and 4FP. It is worth pointing out here that in the case of 2FP, the computed PEC along the O−H stretching coordinate

https://doi.org/10.1021/acsomega.4c11321
ACS Omega 2025, 10, 7389−7399

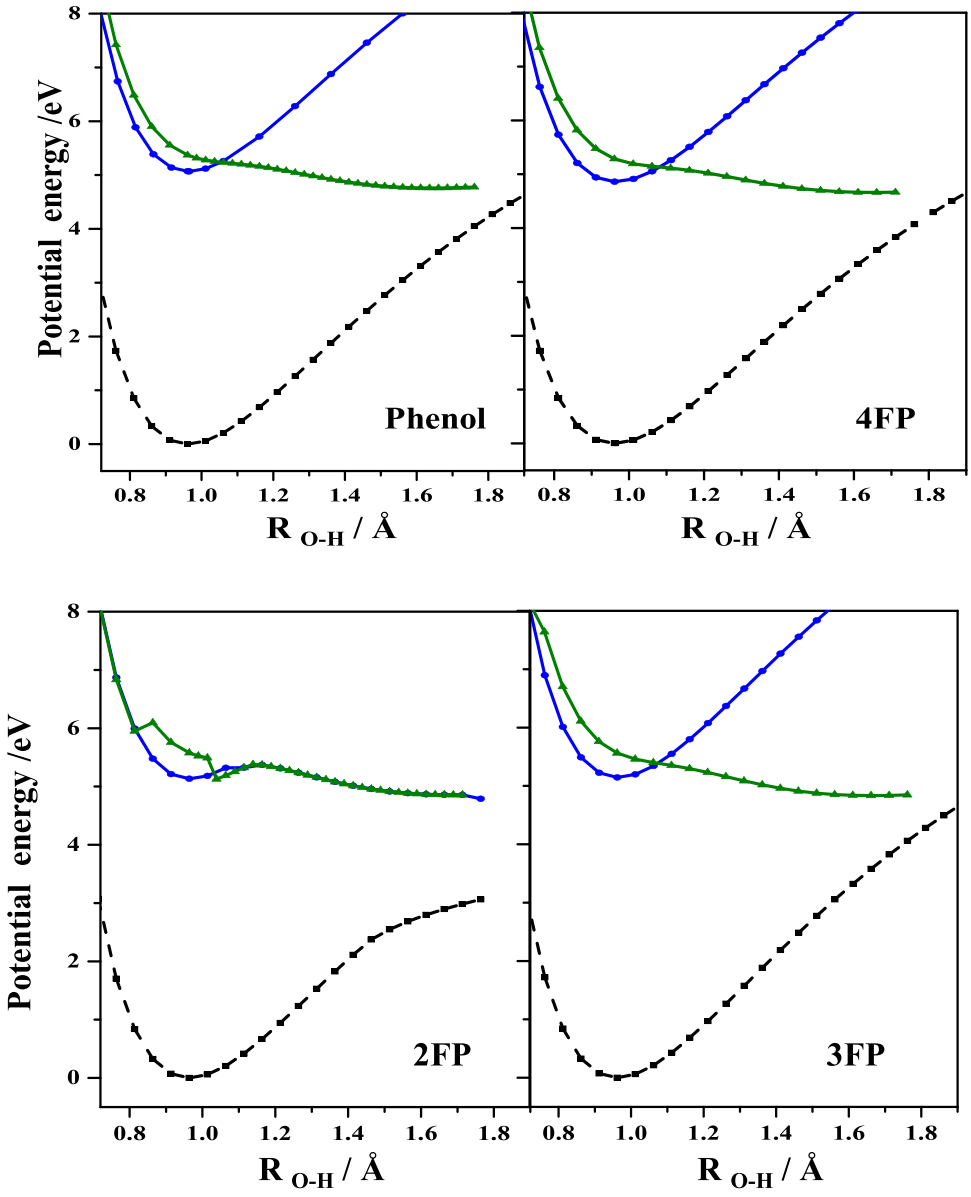

Figure 5. Cuts through the ground (black), first (blue), and second (green) excited singlet PECs of phenol, 4FP, 2FP, and 3FP plotted as functions of the O−H stretching coordinate. Calculations were performed at TDDFT/CAMB3LYP/6-311++G(d,p) level.

looks somewhat distorted, but it is consistent with those of the other reports.[10,93] Earlier, Chatterjee et al. showed experimental evidence for the occurrence of HF eliminations in resonance two-photon ionization mass spectrometry in the S_1 state of the 2FP monomer.[93]

For the aromatic systems, a much-discussed alternative mechanism for the opening-up of the nonradiative decay channel in S_1 is the S_1/S_0 CI with respect to prefulvenic geometric distortion. Evidence for such mechanism was discussed earlier for systems like benzene, phenol, chlorophenol, etc.[76−78,23,80] In the literature, this pathway is known as "channel-three" nonradiative relaxation pathway, and it was proposed to be responsible for the low quantum yield of fluorescence after excitation to higher vibronic levels in S_1 of benzene and substituted benzenes. With sufficient excess energy in S_1, this alternative decay pathway comes into play along with other nonradiative decay mechanisms. The energy barriers to the S_1/S_0 CIs with respect to the S_1 minima for phenol, 2FP, 3FP, and 4FP, calculated at CASSCF/Dunning cc-pVDZ level, are presented in Table 2. The geometric distortions at the S_1/S_0 CI are pictorially depicted in Figure 6.

Table 2. Calculated Energy Barrier for S_1/S_0 CI (in eV) of Phenol, 2FP, 3FP, and 4FP at CASSCF/Dunning cc-pVDZ Level with respect to Prefulvenic Mode

	barrier height to S_1/S_0 CI_{Pref} from S_1 minimum/eV
phenol	0.721
2FP	0.925
3FP	0.188
4FP	0.990

The calculation clearly depicts that while this prefulvenic CI energy barrier is quite high for phenol, 2FP, and 4FP (0.721 eV, 0.925 eV, and 0.990 eV, respectively), the same CI exists at a significantly lower energy barrier of only 0.188 eV for 3FP, which could be readily accessible upon photoexcitation to the $^1\pi\pi^*$ state, and offers an efficient nonradiative relaxation

https://doi.org/10.1021/acsomega.4c11321
ACS Omega 2025, 10, 7389−7399

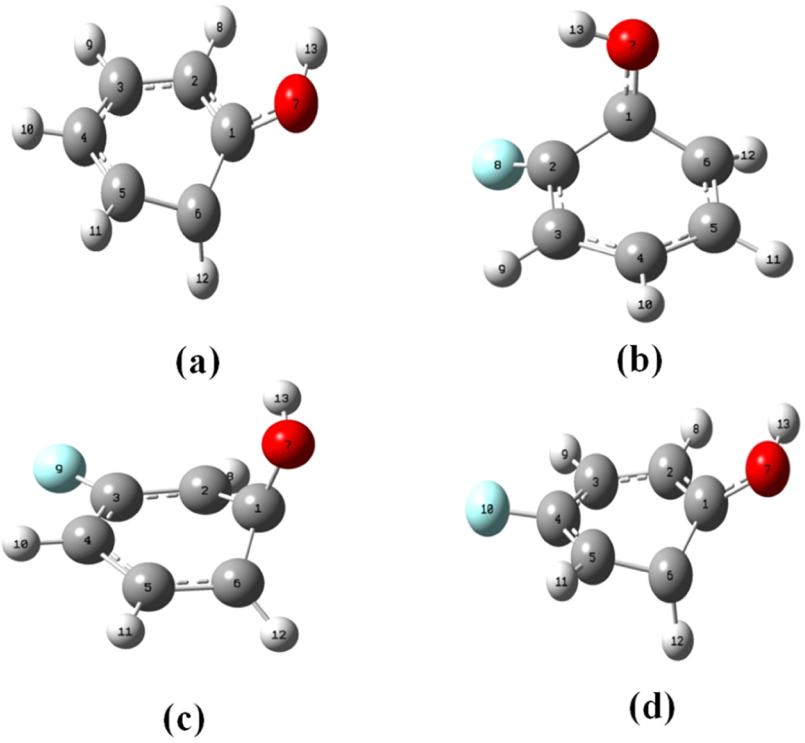

Figure 6. Optimized geometries at S_1/S_0 CIs with respect to the prefulvenic isomerization coordinates of (a) phenol, (b) 2FP, (c) 3FP, and (d) 4FP performed at CASSCF/Dunning cc-pVDZ level of calculation.

pathway to the ground state. Therefore, the S_1/S_0 CI is a likely origin for the significantly diminished fluorescence yield of the molecule.

Selected geometrical parameters at the prefulvenic CI points of phenol, 2FP, 3FP, and 4FP are presented in Table S5 (SI). It is apparent from the presented data that geometric distortion at the CI is a maximum for 3FP.

For 4FP, on the other hand, the extended aromatic conjugation not only results in retention of planarity of the molecule in S_1 but also effectively enhances the S_1/S_0 CI barrier. As a result, the fluorescence yield of 4FP turns out to be maximum among the four molecules discussed here and the same factor is also responsible for lengthening of the excited-state lifetime as reported.[98] The effects of structural rigidity on vibrational relaxation and on nonradiative decay processes are well documented.[98] In the case of 2FP, due to the close proximity of hydrogen and fluorine atoms in *ortho*-conformation, HF loss can occur efficiently upon $S_1 \leftarrow S_0$ electronic excitation in the gas phase.[93] In contrast, in the liquid phase, due to the cageing effect, the HF loss process is hindered.[93] On the other hand, 3FP, having the least π-conjugation, is prone to skeletal distortions and upon $^1\pi\pi^*$ excitation it undergoes out-of-plane ring deformations and follows the relaxation pathway through S_1/S_0 prefulvenic CI.

Displayed in Figure 7 are the potential energy profiles along the ∠C1−C2−C3−C4 dihedral angle of 3FP in the S_1 and S_0 states. In contrast to S_0, the curve is extremely shallow in the S_1 state, resulting in a CI with S_0 state at an angle of around 40°. In Figure 7, the potential energy has been plotted against the extent of out-of-plane ring deformation, where the ∠C1−C2−C3−C4 dihedral angle at the S_1/S_0 CI point has been considered as the maximum out-of-plane ring deformation. The calculated minimum energy path on the relaxed S_1 PEC is essentially barrierless and may cause instantaneous photo-

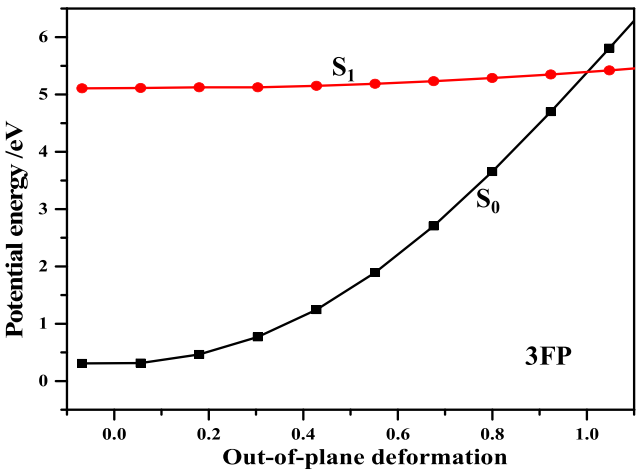

Figure 7. PECs of 3FP along the ∠C1−C2−C3−C4 dihedral angle in the S_0 and S_1 states calculated at the CAMB3LYP/6-311++G(d,p) level. The *x*-axis shows the extent of out-of-plane ring deformation, where the ∠C1−C2−C3−C4 dihedral angle at the S_1/S_0 CI point has been considered as the maximum out-of-plane ring deformation, and the planar geometry corresponds to 0.

relaxation to the ground state, resulting in the exceptionally low fluorescence intensity of 3FP.

4. SUMMARY

In this article, we have reported an investigation of the photophysical behavior of phenol, 2FP, 3FP, and 4FP by means of an integrated approach of UV spectroscopy in a nonpolar liquid and electronic structure theory calculation. In the electronic absorption spectra, the finer vibronic structures of 4FP are very prominent, but those are somewhat diminished in the spectra of 2FP and 3FP and the longest wavelength peak

https://doi.org/10.1021/acsomega.4c11321
ACS Omega 2025, 10, 7389−7399

(electronic origin band) of the $S_1 \leftarrow S_0$ absorption spectra is shifted to longer wavelengths in the order 2FP < 3FP < phenol < 4FP. The most remarkable contrasts in photophysical behavior of phenol, 2FP, 3FP, and 4FP are manifested in the fluorescence spectral bandwidths (FWHM) and the fluorescence yields. The fluorescence bandwidth of 2FP is nearly 1.5 times that of 4FP, whereas the fluorescence yield of 3FP is nearly an order of magnitude smaller than that of 4FP. The electronic structure theory methods used at TDDFT/CAMB3LYP/6-311++G(d,p) and CASSCF/Dunning cc-pVDZ levels offer an interpretation of the electronic origins for the observations and, in particular, the experimentally low yield of 3FP fluorescence. Fluorine atom exerts an electron-withdrawing inductive effect more effectively at *ortho*- and *meta*-positions, but at *para*-position, the electron-releasing mesomeric effect of the same acts dominantly. Electronic structure calculations predict minimal geometric distortions upon photoexcitation to the S_1 state for 4FP and phenol, but for 2FP and 3FP, the extents of geometrical distortions are significantly large, which is quite consistent with the large Stokes shifts of the latter two molecules. A low barrier to S_1/S_0 CI corresponding to the prefulvenic mode has been predicted, which has been considered to be the most efficient nonradiative channel for the effective quenching of 3FP fluorescence.

■ ASSOCIATED CONTENT

Supporting Information

The Supporting Information is available free of charge at https://pubs.acs.org/doi/10.1021/acsomega.4c11321.

> Optimized geometric parameters of phenol in S_0 and S_1 state; optimized geometric parameters of 2-fluorophenol (2FP) in S_0 and S_1 state; optimized geometric parameters of 3-fluorophenol (2FP) in S_0 and S_1 state; optimized geometric parameters of 4-fluorophenol (2FP) in S_0 and S_1 state; optimized geometric parameters of phenol, 2FP, 3FP and 4FP in S_1/S_0 CI point (PDF)

■ AUTHOR INFORMATION

Corresponding Author

Jayshree Sadhukhan − *Department of Chemistry, Government General Degree College, Hooghly 712409 West Bengal, India*; orcid.org/0000-0002-9092-4666; Phone: +91-33-2630-0126; Email: jayshreechemistry@gmail.com

Authors

Moitrayee Mukherjee − *Department of Physics, Rishi Bankim Chandra College, Naihati 743165 West Bengal, India*

Piyali Chatterjee − *School of Applied Science and Humanities, Haldia Institute of Technology, Haldia 721657 West Bengal, India*

Anwesha Datta − *School of Chemical Sciences, Indian Association for the Cultivation of Science, Kolkata 700032, India*

Complete contact information is available at: https://pubs.acs.org/10.1021/acsomega.4c11321

Notes

The authors declare no competing financial interest.

■ ACKNOWLEDGMENTS

J.S. sincerely thanks the Department of Science and Technology and Biotechnology, Govt. of West Bengal for a minor research project grant, no. 1358(Sanc.)/STBT-11012(25)/47/2021-ST SEC. P.C. thanks the SERB, project no. CRG/2022/005451, Govt. of India for providing the needful financial support to carry out this experimental research work. A.D. thanks IACS, Kolkata for the Senior Research Fellowship. The authors sincerely thank Subhasis Mandal for his assistance and Prof. T. Chakraborty and Prof. S. Adhikari for valuable discussion and guidance.

■ REFERENCES

(1) Born, M.; Oppenheimer, R. Zur Quantentheorie der Molekeln. *Ann. Phys.* **1927**, *389*, 457−484.

(2) Köppel, H.; Domcke, W.; Cederbaum, L. S. *Adv. Chem. Phys.* **1984**, *57*, 59−246.

(3) Bersuker, B.; Polinger, V. Z. *Vibronic Interactions in Molecules and Crystals*; Springer-Verlag: Berlin-Heidelberg-New York, 1989.

(4) *Conical Intersections: Electronic Structure, Dynamics and Spectroscopy*; Domcke, W.; Yarkony, D. R.; Köppel, H., Eds.; World Scientific: Singapore, 2004.

(5) *Conical Intersections: Theory, Computation and Experiment*; Domcke, W.; Yarkony, D. R.; Köppel, H., Eds.; World Scientific: Singapore, 2011.

(6) Domcke, W.; Yarkony, D. R. Role of Conical Intersections in Molecular Spectroscopy and Photoinduced Chemical Dynamics. *Annu. Rev. Phys. Chem.* **2012**, *63*, 325−352.

(7) Worth, G. A.; Cederbaum, L. S. Beyond Born-Oppenheimer: molecular dynamics through a conical intersection. *Annu. Rev. Phys. Chem.* **2004**, *55*, 127−158.

(8) Mahapatra, S. Quantum non-adiabatic dynamics through conical intersections: Spectroscopy to reactive scattering. *Int. Rev. Phys. Chem.* **2004**, *23*, 483−512.

(9) Ramos, R.; Spierings, D.; Racicot, I.; Steinberg, A. M. Measurement of the time spent by a tunnelling atom within the barrier region. *Nature* **2020**, *583*, 529−532.

(10) Deng, X.; Tang, Y.; Song, X.; Liu, K.; Gu, Z.; Zhang, B. Photolysis dynamics of m- and o-fluorophenol: Substitution effects on tunneling mechanism. *Chemosphere* **2020**, *253*, No. 126747.

(11) Roberts, G. M.; Stavros, V. G. The role of $\pi\sigma^*$ states in the photochemistry of heteroaromatic biomolecules and their subunits: insights from gas-phase femtosecond spectroscopy. *Chem. Sci.* **2014**, *5*, 1698−1722.

(12) Young, J. D.; Staniforth, M.; Dean, J. C.; Roberts, G. M.; Mazzoni, F.; Karsili, T. N. V.; Ashfold, M. N. R.; Zwier, T. S.; Stavros, V. G. Towards Understanding Photodegradation Pathways in Lignins: The Role of Intramolecular Hydrogen Bonding in Excited States. *J. Phys. Chem. Lett.* **2014**, *5*, 2138−2143.

(13) Roberts, G. M.; Chatterley, A. S.; Young, J. D.; Stavros, V. G. Direct Observation of Hydrogen Tunneling Dynamics in Photoexcited Phenol. *J. Phys. Chem. Lett.* **2012**, *3*, 348−352.

(14) Woo, K. C.; Kim, S. K. Multidimensional H Atom Tunneling Dynamics of Phenol: Interplay between Vibrations and Tunneling. *J. Phys. Chem. A* **2019**, *123*, 1529−1537.

(15) Marchetti, B.; Karsili, T. N. V.; Cipriani, M.; Hansen, C. S.; Ashfold, M. N. R. The near ultraviolet photodissociation dynamics of 2- and 3-substituted thiophenols: Geometric vs. electronic structure effects. *J. Chem. Phys.* **2017**, *147*, No. 013923.

(16) Horbury, M. D.; Baker, L. A.; Quan, W. D.; Young, J. D.; Staniforth, M.; Greenough, S. E.; Stavros, V. G. Bridging the Gap between the Gas Phase and Solution Phase: Solvent Specific Photochemistry in 4-tert-Butylcatechol. *J. Phys. Chem. A* **2015**, *119*, 11989−11996.

(17) Han, S.; You, H. S.; Kim, S. Y.; Kim, S. K. Dynamic Role of the Intramolecular Hydrogen Bonding in Nonadiabatic Chemistry Revealed in the UV Photodissociation Reactions of 2- Fluorothio-

phenol and 2-Chlorothiophenol. *J. Phys. Chem. A* **2014**, *118*, 6940−6949.
(18) Karsili, T. N. V.; Wenge, A. M.; Marchetti, B.; Ashfold, M. N. R. Symmetry matters: photodissociation dynamics of symmetrically versus asymmetrically substituted phenols. *Phys. Chem. Chem. Phys.* **2014**, *16*, 588−598.
(19) Chatterley, A. S.; Young, J. D.; Townsend, D.; Żurek, J. M.; Paterson, M. J.; Roberts, G. M.; Stavros, V. G. Manipulating dynamics with chemical structure: probing vibrationally enhanced tunnelling in photoexcited catechol. *Phys. Chem. Chem. Phys.* **2013**, *15*, 6879−6892.
(20) Hadden, D. J.; Roberts, G. M.; Karsili, T. N. V.; Ashfold, M. N. R.; Stavros, V. G. Competing 1$\pi\sigma$* mediated dynamics in mequinol: O−H versus O−CH3 photodissociation pathways. *Phys. Chem. Chem. Phys.* **2012**, *14*, 13415−13428.
(21) King, G. A.; Oliver, T. A. A.; Dixon, R. N.; Ashfold, M. N. R. Vibrational energy redistribution in catechol during ultraviolet photolysis. *Phys. Chem. Chem. Phys.* **2012**, *14*, 3338−3345.
(22) Pino, G. A.; Oldani, A. N.; Marceca, E.; Fujii, M.; Ishiuchi, S.-I.; Miyazaki, M.; Broquier, M.; Dedonder, C.; Jouvet, C. Excited state hydrogen transfer dynamics in substituted phenols and their complexes with ammonia: $\pi\pi^*$-$\pi\sigma^*$ energy gap propensity and ortho-substitution effect. *J. Chem. Phys.* **2010**, *133*, No. 124313.
(23) Vieuxmaire, O. P. J.; Lan, Z.; Sobolewski, A. L.; Domcke, W. Ab initio characterization of the conical intersections involved in the photochemistry of phenol. *J. Chem. Phys.* **2008**, *129*, No. 224307.
(24) Tseng, C. M.; Lee, Y. T.; Ni, C. K. H atom elimination from the $\pi\sigma^*$ state in the photodissociation of phenol. *J. Chem. Phys.* **2004**, *121*, 2459−2461.
(25) Ashfold, M. N. R.; Cronin, B.; Devine, A. L.; Dixon, R. N.; Nix, M. G. D. The role of $\pi\sigma^*$ excited states in the photodissociation of heteroaromatic molecules. *Science* **2006**, *312*, 1637−1640.
(26) Sobolewski, A. L.; Domcke, W.; Dedonder-Lardeux, C.; Jouvet, C. Excited-state hydrogen detachment and hydrogen transfer driven by repulsive $^1\pi\sigma^*$ states: A new paradigm for nonradiative decay in aromatic biomolecules. *Phys. Chem. Chem. Phys.* **2002**, *4*, 1093−1100.
(27) Sobolewski, A. L.; Domcke, W. Conical intersections induced by repulsive $^1\pi\sigma^*$ states in planar organic molecules: malonaldehyde, pyrrole and chlorobenzene as photochemical model systems. *Chem. Phys.* **2000**, *259*, 181−191.
(28) Lan, Z.; Domcke, W.; Vallet, V.; Sobolewski, A. L.; Mahapatra, S. Time-dependent quantum wave-packet description of the $^1\pi\sigma^*$ photochemistry of phenol. *J. Chem. Phys.* **2005**, *122*, No. 224315.
(29) Vallet, V.; Lan, Z.; Mahapatra, S.; Sobolewski, A. L.; Domcke, W. Time-dependent quantum wave-packet description of the $^1\pi\sigma^*$ photochemistry of pyrrole. *Faraday Discuss.* **2004**, *127*, 283−293.
(30) Sala, M. *Quantum Dynamics and Laser Control for Photochemistry*; Springer International Publishing: Cham, 2016; p 87.
(31) Sala, M.; Lasorne, B.; Gatti, F.; Guerin, S. The role of the low-lying dark nπ^* states in the photophysics of pyrazine: a quantum dynamics study. *Phys. Chem. Chem. Phys.* **2014**, *16*, 15957−15967.
(32) Lee, J. K.; Fujiwara, T.; Kofron, W. G.; Zgierski, M. Z.; Lim, E. C. The low-lying$\pi\sigma^*$ state and its role in the intramolecular charge transfer of aminobenzonitriles and aminobenzethyne. *J. Chem. Phys.* **2008**, *128*, No. 164512.
(33) Loper, G. L.; Lee, E. K. C. Fluorescence decay and radiative lifetimes of fluorinated aromatic molecules. *Chem. Phys. Lett.* **1972**, *13*, 140−143.
(34) Tseng, C. M.; Lee, Y. T.; Lin, M. F.; Ni, C. K.; Liu, S. Y.; Lee, Y. P.; Xu, Z. F.; Lin, M. C. Photodissociation dynamics of Phenol. *J. Phys. Chem. A* **2007**, *111*, 9463−9470.
(35) Devine, A. L.; Nix, M. G. D.; Cronin, B.; Ashfold, M. N. R. Near-UV photolysis of substituted phenols, I: 4-fluoro-, 4-chloro- and 4-bromophenol. *Phys. Chem. Chem. Phys.* **2007**, *9*, 3749−3762.
(36) King, G. A.; Devine, A. L.; Nix, M. G. D.; Kelly, D. E.; Ashfold, M. N. R. Near-UV photolysis of substituted phenols Part II. 4-, 3- and 2-methylphenol. *Phys. Chem. Chem. Phys.* **2008**, *10*, 6417−6429.
(37) Cronin, B.; Nix, M. G. D.; Qadiri, R. H.; Ashfold, M. N. R. High resolution photofragment translational spectroscopy studies of the near ultraviolet photolysis of pyrrole. *Phys. Chem. Chem. Phys.* **2004**, *6*, 5031−5041.
(38) Lan, Z.; Domcke, W. Role of vibrational energy relaxation in the photoinduced nonadiabatic dynamics of pyrrole at the $^1\pi\sigma^* - S_0$ conical intersection. *Chem. Phys.* **2008**, *350*, 125−138.
(39) Lan, Z.; Du pays, A.; Vallet, V.; Mahapatra, S.; Domcke, W. Photoinduced multi-mode quantum dynamics of pyrrole at the 1$\pi\sigma^*$ - S_0 conical intersections. *J. Photochem. Photobiol., A* **2007**, *190*, 177−189.
(40) Nix, M. G. D.; Devine, A. L.; Cronin, B.; Dixon, R. N.; Ashfold, M. N. R. High resolution photofragment translational spectroscopy studies of the near ultraviolet photolysis of phenol. *J. Chem. Phys.* **2006**, *125*, No. 133318.
(41) Mondal, T.; Mahapatra, S. Photophysics of fluorinated benzene. I. Quantum chemistry. *J. Chem. Phys.* **2010**, *133*, No. 084304.
(42) Mondal, T.; Mahapatra, S. Photophysics of fluorinated benzene. II. Quantum dynamics. *J. Chem. Phys.* **2010**, *133*, No. 084305.
(43) Mondal, T.; Reddy, S. R.; Mahapatra, S. Photophysics of fluorinated benzene. III. Hexafluorobenzene. *J. Chem. Phys.* **2012**, *137*, No. 054311.
(44) Mondal, T.; Mahapatra, S. The Jahn−Teller and pseudo-Jahn−Teller effects in the low-lying electronic states of 1,3,5-trifluorobenzene radical cation. *Phys. Chem. Chem. Phys.* **2009**, *11*, 10867−10880.
(45) Philis, J. G.; Mondal, T.; Mahapatra, S. Vibronic structure in the low lying Rydberg states of hexafluorobenzene and 1,3,5-trifluorobenzene detected by two-photon spectroscopy. *Chem. Phys. Lett.* **2010**, *495*, 187−191.
(46) Cooper, G. A.; Cobbin, M. R.; Ashfold, M. N. R. Effects of ring fluorination on the ultraviolet photodissociation dynamics of Phenol. *J. Phys. Chem. A* **2020**, *124* (47), 9698−9709.
(47) Roberts, G. M.; Chatterley, A. S.; Young, J. D.; Stavros, V. G. Direct Observation of Hydrogen Tunneling Dynamics in Photoexcited Phenol. *J. Phys. Chem. Lett.* **2012**, *3*, 348−352.
(48) Lakowicz, J. R. *Principle of Fluorescence Spectroscopy*, 3rd ed.; Springer: New York, 2006.
(49) Biswas, P.; Pandey, P.; Chakraborty, T. Dispersed fluorescence spectroscopy of p-fluorophenol. *Chem. Phys. Lett.* **2008**, *454*, 163−170.
(50) Jones, D. B.; da Silva, G. B.; Neves, R. F. C.; Duque, H. V.; Chiari, L.; de Oliveira, E. M.; Lopes, M. C. A.; da Costa, R. F.; Varella, M. T.; Bettega, M. H. F.; Lima, M. A. P.; Brunger, M. J. An experimental and theoretical investigation into the excited electronic states of phenol. *J. Chem. Phys.* **2014**, *141*, No. 074314.
(51) Zwier, T. S. The Spectroscopy of solvation in hydrogen-bonded aromatic clusters. *Annu. Rev. Phys. Chem.* **1996**, *47*, 205−241.
(52) Sobolewski, A. L.; Domcke, W. Photoinduced electron and proton transfer in Phenol and its clusters with water and ammonia. *J. Phys. Chem. A* **2001**, *105*, 9275−9283.
(53) Mukhopadhyay, D. P.; Biswas, S.; Chakraborty, T. LIF spectroscopy of p-Fluorophenol···Water complex: hydrogen bond vibrations, fermi Resonance, and vibrational relaxation in the excited state. *J. Phys. Chem. A* **2016**, *120* (46), 9159−9169.
(54) Ishiuchi, S. I.; Kamizori, J.; Tsuji, N.; Sakai, M.; Miyazaki, M.; Dedonder, C.; Jouvet, C.; Fujii, M. Excited state hydrogen transfer dynamics in phenol−$(NH_3)_2$ studied by picosecond UV-near IR-UV time-resolved spectroscopy. *Phys. Chem. Chem. Phys.* **2020**, *22*, 5740−5748.
(55) Bent, D. V.; Hayon, E. Excited state chemistry of aromatic amino acids and related peptides. III. Tryptophan. *J. Am. Chem. Soc.* **1975**, *97*, 2612−2619.
(56) Zechner, J.; Köhler, G.; Grabner, G.; Getoff, N. Excitation energy dependence of the quantum yields of fluorescence and electron formation from aqueous phenol by means of the heavy atom effect. *Chem. Phys. Lett.* **1976**, *37*, 297−300.
(57) Zechner, J.; Kohler, G.; Grabner, G.; Getoff, N. The role of the molecular environment for the primary photoprocesses of phenol in solution. *Can. J. Chem.* **1980**, *58*, 2006−2010.

https://doi.org/10.1021/acsomega.4c11321
ACS Omega 2025, 10, 7389−7399

(58) Mialocq, J. C.; Sutton, J.; Goujon, P. Picosecond study of electron ejection in aqueous phenol and phenolate solutions. *J. Chem. Phys.* **1980**, *72*, 6338−6345.
(59) Grabner, G.; Koehler, G.; Zechner, J.; Getoff, N. Temperature dependence of photoprocesses in aqueous phenol. *J. Phys. Chem. A* **1980**, *84*, 3000−3004.
(60) Dellonte, S.; Marconi, G. Temperature effects on the photophysical behaviour of phenol and anisole in various solvents. *J. Photochem.* **1985**, *30*, 37−46.
(61) Karmakar, S.; Mukhopadhyay, D. P.; Chakraborty, T. Electronic spectra and excited state dynamics of pentafluorophenol: Effects of low-lying $\pi\sigma^*$ states. *J. Chem. Phys.* **2015**, *142*, No. 184303.
(62) Creed, D. The Photophysics and Photochemistry of the near-UV absorbing amino acids−II. Tyrosine and its simple derivatives. *Photochem. Photobiol.* **1984**, *39*, 563−575.
(63) Lipert, R. J.; Bermudez, G.; Colson, S. D. Pathways of S_1 decay in phenol, indoles, and water complexes of phenol and indole in a free jet expansion. *J. Phys. Chem. A* **1988**, *92*, 3801−3805.
(64) Domcke, W.; Sobolewski, A. L. Unraveling the molecular mechanisms of photoacidity. *Science* **2003**, *302*, 1693−1694.
(65) Xie, C.; Ma, J.; Zhu, X.; Yarkony, D. R.; Xie, D.; Guo, H. Nonadiabatic tunneling in photodissociation of Phenol. *J. Am. Chem. Soc.* **2016**, *138*, 7828−7831.
(66) Xu, X.; Zheng, J.; Yang, K. R.; Truhlar, D. G. Photodissociation dynamics of Phenol: multistate trajectory simulations including tunneling. *J. Am. Chem. Soc.* **2014**, *136*, 16378−16386.
(67) Hause, M. L.; Yoon, Y. H.; Case, A. S.; Crim, F. F. Dynamics at conical intersections: The influence of O−H stretching vibrations on the photodissociation of phenol. *J. Chem. Phys.* **2008**, *128*, No. 104307.
(68) Lipert, R. J.; Colson, S. D. Deuterium isotope effects on S_1 radiationless decay in phenol and on intermolecular vibrations in the phenol-water complex. *J. Phys. Chem. A* **1989**, *93*, 135.
(69) Ebata, T.; Mizuochi, N.; Watanabe, T.; Mikami, N. OH Stretching Vibrations of Phenol−$(H_2O)_1$ and Phenol−$(H_2O)_3$ in the S_1 State. *J. Phys. Chem. A* **1996**, *100*, 546−550.
(70) Schick, C. P.; Carpenter, S. D.; Weber, P. M. Femtosecond multiphoton ionization photoelectron spectroscopy of the S_2 state of Phenol. *J. Phys. Chem. A* **1999**, *103*, 10470−10476.
(71) Ebata, T.; Iwasaki, A.; Mikami, N. Vibrational relaxation of OH and OD stretching vibrations of Phenol and its clusters studied by IR-UV pump-probe spectroscopy. *J. Phys. Chem. A* **2000**, *104*, 7974−7979.
(72) Kayano, M.; Ebata, T.; Yamada, Y.; Mikami, N. Picosecond IR−UV pump−probe spectroscopic study of the dynamics of the vibrational relaxation of jet-cooled phenol. II. Intracluster vibrational energy redistribution of the OH stretching vibration of hydrogen-bonded clusters. *J. Chem. Phys.* **2004**, *120*, 7410−7417.
(73) Livingstone, R. A.; Thompson, J. O. F.; Iljina, M.; Donaldson, R. J.; J Sussman, B.; Paterson, M. J.; Townsend, D. Time-resolved photoelectron imaging of excited state relaxation dynamics in phenol, catechol, resorcinol, and hydroquinone. *J. Chem. Phys.* **2012**, *137*, No. 184304.
(74) Ashfold, M. N. R.; King, G. A.; Murdock, D.; Nix, M. G. D.; Oliver, T. A. A.; Sage, A. G. $\pi\sigma^*$ excited states in molecular photochemistry. *Phys. Chem. Chem. Phys.* **2010**, *12*, 1218−1238.
(75) An, H.; Baeck, K. K. Quantum Wave Packet Propagation Study of the Photochemistry of Phenol: Isotope Effects (Ph-OD) and the Direct Excitation to the $1\pi\sigma^*$ state. *J. Phys. Chem. A* **2011**, *115*, 13309−13315.
(76) Kato, S. A theoretical study on the mechanism of internal conversion of S_1 benzene. *J. Chem. Phys.* **1988**, *88*, 3045−3056.
(77) Palmer, I. J.; Ragazos, I. N.; Bernardi, F.; Olivucci, M.; Robb, M. An MC-SCF study of the S_1 and S_2 photochemical reactions of benzene. *J. Am. Chem. Soc.* **1993**, *115*, 673−682.
(78) Sobolewski, A. L.; Woywod, C.; Domcke, W. Ab initio investigation of potential-energy surfaces involved in the photophysics of benzene and pyrazine. *J. Chem. Phys.* **1993**, *98*, 5627−5641.
(79) Sage, A. G.; Oliver, T. A. A.; King, G. A.; Murdock, D.; Harvey, J. N.; Ashfold, M. N. R. UV Photolysis of 4-Iodo-, 4-Bromo-, and 4-Chlorophenol: Competition between C−Y (Y = Halogen) and O−H Bond Fission. *J. Chem. Phys.* **2013**, *138*, No. 164318.
(80) Harris, S. J.; Karsili, T. N. V.; Murdock, D.; Oliver, T. A. A.; Wenge, A. M.; Zaouris, D. K.; Ashfold, M. N. R.; Harvey, J. N.; Few, J. D.; Gowrie, S.; Hancock, G.; Hadden, D. J.; Roberts, G. M.; Stavros, V. G.; Spighi, G.; Poisson, L.; Soep, B. A Multipronged Comparative Study of the Ultraviolet Photochemistry of 2-, 3-, and 4-Chlorophenol in the Gas Phase. *J. Phys. Chem. A* **2015**, *119*, 6045−6056.
(81) Brundle, C. R.; Robin, M. B.; Kuebler, N. A. Perfluoro Effect in Photoelectron Spectroscopy. II. Aromatic Molecules. *J. Am. Chem. Soc.* **1972**, *94* (5), 1466−1475.
(82) Philis, J.; Bolovinos, A.; Andritsopoulos, G.; Pantos, E.; Tsekeris, P. A comparison of the absorption spectra of the fluorobenzenes and Benzene in the region 4.5−9.5 eV. *J. Phys. B* **1981**, *14* (19), 3621−3635.
(83) Zgierski, M. Z.; Fujiwara, T.; Lim, E. C. Photophysics of aromatic molecules with low-lying $\pi\sigma^*$ states: fluorinated Benzenes. *J. Chem. Phys.* **2005**, *122* (14), No. 144312.
(84) Han, J.; Tao, F.-M. Correlations and Predictions of pKa Values of Fluorophenols and Bromophenols Using Hydrogen-Bonded Complexes with Ammonia. *J. Phys. Chem. A* **2006**, *110* (1), 257−263.
(85) Rajak, K.; Ghosh, A.; Mahapatra, S. Photophysics of Phenol and Pentafluorophenol: The Role of Nonadiabaticity in the Optical Transition to the Lowest Bright $^1\pi\pi^*$ State. *J. Chem. Phys.* **2018**, *148* (5), No. 054301.
(86) Winslow, M.; Cross, W. B.; Robinson, D. Comparison of spin-flip TDDFT-based conical intersection approaches with XMS-CASPT2. *J. Chem. Theory Comput.* **2020**, *16*, 3253−3263.
(87) Levine, B. G.; Ko, C.; Quenneville, J.; MartÍnez, T. J. Conical intersections and double excitations in time-dependent density functional theory. *Mol. Phys.* **2006**, *104*, 1039−1051.
(88) Filatov, M. Assessment of Density Functional Methods for Obtaining Geometries at Conical Intersections in Organic Molecules. *J. Chem. Theory Comput.* **2013**, *9*, 4526−4541.
(89) Fantacci, S.; Migani, A.; Olivucci, M. CASPT2//CASSCF and TDDFT//CASSCF mapping of the excited state isomerization path of a minimal model of the retinal chromophore. *J. Phys. Chem. A* **2004**, *108*, 1208−1213.
(90) Savarese, M.; Raucci, U.; Fukuda, R.; Adamo, C.; Ehara, M.; Rega, N.; Ciofini, I. Comparing the performance of TD-DFT and SAC-CI methods in the description of excited states potential energy surfaces: An excited state proton transfer reaction as case study. *J. Comput. Chem.* **2017**, *38*, 1084−1092.
(91) Savarese, M.; Raucci, U.; Adamo, C.; Netti, P. A.; Ciofinic, I.; Rega, N. Non-radiative decay paths in rhodamines: new theoretical insights. *Phys. Chem. Chem. Phys.* **2014**, *16*, 20681−20688.
(92) Jacquemin, D.; Perpe′te, E. A.; Ciofini, I.; Adamo, C.; Valero, R.; Zhao, Y.; Truhlar, D. G. On the Performances of the M06 Family of Density Functionals for Electronic Excitation Energies. *J. Chem. Theory Comput.* **2010**, *6*, 2071−2085.
(93) Chatterjee, P.; Ghosh, A. K.; Chakraborty, T. Hydrogen bond induced HF elimination from photoionized fluorophenol dimers in the gas phase. *J. Chem. Phys.* **2017**, *146*, No. 084310.
(94) Frisch, M. J.; Trucks, G. W.; Schlegel, H. B.; Scuseria, G. E.; Robb, M. A.; Cheeseman, J. R.; Scalmani, G.; Barone, V.; Mennucci, B.; Petersson, G. A.; Nakatsuji, H.; Caricato, M.; Li, X.; Hratchian, H. P.; Izmaylov, A. F.; Bloino, J.; Zheng, G.; Sonnenberg, J. L.; Hada, M.; Ehara, M.; Toyota, K.; Fukuda, R.; Hasegawa, J.; Ishida, M.; Nakajima, T.; Honda, Y.; Kitao, O.; Nakai, H.; Vreven, T.; Montgomery, J. A., Jr.; Peralta, J. E.; Ogliaro, F.; Bearpark, M.; Heyd, J. J.; Brothers, E.; Kudin, K. N.; Staroverov, V. N.; Kobayashi, R.; Normand, J.; Raghavachari, K.; Rendell, A.; Burant, J. C.; Iyengar, S. S.; Tomasi, J.; Cossi, M.; Rega, N.; Millam, J. M.; Klene, M.; Knox, J. E.; Cross, J. B.; Bakken, V.; Adamo, C.; Jaramillo, J.; Gomperts, R.; Stratmann, R. E.; Yazyev, O.; Austin, A. J.; Cammi, R.; Pomelli, C.; Ochterski, J. W.; Martin, R. L.; Morokuma, K.; Zakrzewski, V. G.; Voth, G. A.; Salvador, P.; Dannenberg, J. J.; Dapprich, S.; Daniels, A.

https://doi.org/10.1021/acsomega.4c11321
ACS Omega 2025, 10, 7389−7399

D.; Farkas, O.; Foresman, J. B.; Ortiz, J. V.; Cioslowski, J.; Fox, D. J. *Gaussian 09*, revision B.01; Gaussian Inc.: Wallingford, 2010.
(95) Schmidt, M. W.; Baldridge, K. K.; Boatz, J. A.; Elbert, S. T.; Gordon, M. S.; Jensen, J. H.; Koseki, S.; Matsunaga, N.; Nguyen, K. A.; Su, S. J.; Windus, T. L.; Dupuis, M.; Montgomery, J. A. General atomic and molecular electronic structure system. *J. Comput. Chem.* **1993**, *14*, 1347−1363.
(96) Tomasi, J.; Mennucci, B.; Cammi, R. Quantum Mechanical Continuum Solvation Models. *Chem. Rev.* **2005**, *105*, 2999−3094.
(97) Ling, F.; Li, S.; Song, X.; Wang, Y.; Long, J.; Zhang, B. Femtosecond time-resolved observation of butterfly vibration in electronically excited *o*-fluorophenol. *Sci. Rep.* **2017**, *7*, No. 15362.
(98) Dai, J.; Zhang, X. Chemical Regulation of Fluorescence Lifetime. *Chem. Biomed. Imaging* **2023**, *1* (9), 796−816.
(99) Berden, G.; Meerts, W. L.; Schmitt, M.; Kleinermanns, K. High resolution UV spectroscopy of phenol and the hydrogen bonded phenol-water cluster. *J. Chem. Phys.* **1996**, *104*, 972−982.
(100) Remmers, K.; Meerts, W. L.; Zehnacker-Rentien, A.; Barbu, K. L.; Lahmani, F. Structural information on the and state of *o*-fluorophenol by hole burning and high resolution ultraviolet spectroscopy. *J. Chem. Phys.* **2000**, *112*, 6237−6244.
(101) Biswas, S.; Bhattacharya, I.; Chakraborty, T. Identification of an emitting metastable state of p-fluorophenol-ammonia 1:2 complex by laser-induced fluorescence spectroscopy. *J. Phys. Chem. A* **2019**, *123*, 10563−10570.
(102) Hollas, J. M. *Modern Spectroscopy*, 4th ed.; Jon Wiley & Sons Ltd: England, 2004; p 33.
(103) Dixon, R. N.; Oliver, T. A. A.; Ashfold, M. N. R. Tunnelling under a conical intersection: Application to the productvibrational state distributions in the UV photodissociation of phenols. *J. Chem. Phys.* **2011**, *134*, No. 194303.

https://doi.org/10.1021/acsomega.4c11321
ACS Omega 2025, 10, 7389−7399